Quantum Storage of Heralded Single Photons in a Praseodymium-Doped Crystal

Daniel Rieländer,[1] Kutlu Kutluer,[1] Patrick M. Ledingham,[1] Mustafa Gündoğan,[1] Julia Fekete,[1*] Margherita Mazzera,[1,†] and Hugues de Riedmatten[1,2]

[1]*ICFO-Institut de Ciencies Fotoniques, Mediterranean Technology Park, 08860 Castelldefels (Barcelona), Spain*

[2]*ICREA-Institució Catalana de Recerca i Estudis Avançats, 08015 Barcelona, Spain*

(Received 17 October 2013; published 31 January 2014)

We report on experiments demonstrating the reversible mapping of heralded single photons to long-lived collective optical atomic excitations stored in a $Pr^{3+}:Y_2SiO_5$ crystal. A cavity-enhanced spontaneous down-conversion source is employed to produce widely nondegenerate narrow-band (≈2 MHz) photon pairs. The idler photons, whose frequency is compatible with telecommunication optical fibers, are used to herald the creation of the signal photons, compatible with the Pr^{3+} transition. The signal photons are stored and retrieved using the atomic frequency comb protocol. We demonstrate storage times up to 4.5 μs while preserving nonclassical correlations between the heralding and the retrieved photon. This is more than 20 times longer than in previous realizations in solid state devices, and implemented in a system ideally suited for the extension to spin-wave storage.

DOI: 10.1103/PhysRevLett.112.040504 PACS numbers: 03.67.Hk, 42.50.Ex, 42.50.Gy, 42.50.Md

Many protocols in quantum information science rely on the efficient and reversible interaction between photons and matter [1]. The interaction lays the basis for the realization of quantum memories for light and of their application, e.g., in quantum repeaters [2,3]. Possible choices for the system used to store light are single atoms in cavities [4], cold or hot atomic gases [5–13], or rare earth (RE) doped solid state systems [14]. Thanks to the weak interaction between the optical active ions and the environment, RE doped crystals offer, when cryogenically cooled, the long optical and spin coherence times typical of atomic systems, free of the drawbacks deriving from atomic motion [15]. Moreover they possess the benefits of the solid state systems, such as strong interaction with light, allowing for efficient storage of photons [16,17], and the prospect for integrated devices. Furthermore, their inhomogeneously broadened absorption lines can be tailored in appropriate structures, like atomic frequency combs (AFCs), to enable storage protocols with remarkable properties (e.g., temporal or frequency multiplexing) [18–24].

Single photon level weak coherent pulses [25,26] and qubits [18,27,28] have been stored in the excited state of rare-earth doped crystals using the AFC scheme. This has recently been extended to the ground state, in the regime of a few photons per pulse [29]. The storage of nonclassical light generated by spontaneous parametric down-conversion (SPDC) has also been demonstrated and has enabled entanglement between one photon and one collective optical atomic excitation in a crystal [30,31], entanglement between two crystals [32], and single photon qubit storage [33,34]. However, the mapping of nonclassical light using AFCs in rare earth doped crystals was obtained so far only in systems with two ground state levels, thus inherently limited to the optical coherence and not directly extendable to spin-wave storage.

On the contrary, Pr^{3+} or Eu^{3+} doped crystals have the required level structure for spin-wave storage [22,23,29].

In particular, $Pr^{3+}:Y_2SiO_5$ is one of the optical memories with the best demonstrated properties. Storage efficiencies as high as 69% for weak coherent states [16] and storage times up to 1 minute (the longest in any system so far) for classical images [35] have been reported. Despite these extraordinary performances, which make $Pr^{3+}:Y_2SiO_5$ an excellent candidate for quantum memories, the storage of quantum light has never been achieved in this material. As a matter of fact, the pseudoquadrupolar interaction which splits the crystal-field singlets into hyperfine sublevels, providing the three-fold ground state required for the storage in the spin state, also establishes a tight bound (< 4 MHz) to the bandwidth of the single photons to be stored. Recently, a SPDC source was developed to create ultranarrow-band photon pairs, with the signal and the idler photons compatible with the Pr^{3+} transition at 606 nm and with telecommunication optical fibers, respectively [36].

In this Letter we report on experiments where one photon of the pair (signal), whose presence is heralded by the other photon (idler), is stored as a collective optical atomic excitation in a $Pr^{3+}:Y_2SiO_5$ crystal with the AFC protocol. We show that the nonclassical correlation between the two photons is preserved for storage times up to 4.5 μs, more than 20 times longer than in previous solid state experiments [30,31]. The demonstrated nonclassical correlations between an atomic excitation stored in a crystal and a photon at telecommunication wavelengths are an essential resource to generate heralded entanglement between remote crystals [37].

The AFC scheme [19] relies on the creation of a series of narrow absorbing peaks with periodicity Δ in a transparency window created within the inhomogeneous profile of the crystal. The single photon is then mapped onto the

crystal, leading, in the ideal case, to a single collective optical excitation: $\sum_{j=1}^{N_A} e^{-i\vec{k}_p\cdot\vec{x}_j} e^{-i\delta_j t}|g_1 \cdots e_j \cdots g_{N_A}\rangle$, where N_A is the number of atoms, $|g\rangle$ and $|e\rangle$ are the ground and excited state, respectively, $\vec{k}_p$ is the single photon wave vector, and $\vec{x}_j$ (δ_j) is the position (detuning) of atom j. After an initial inhomogeneous dephasing, the atoms will rephase after a time $\tau = 1/\Delta$ giving rise to a reemission of the photon in the forward direction, the so called AFC echo [18].

Figure 1(a) represents the experimental setup. The coherent light at 606 nm is obtained by sum frequency generation of 1570 nm and 987 nm lasers [23]. Its frequency is locked to a temperature stabilized cavity placed in a home-made vacuum chamber. Two beams are spatially separated, the first being used as a frequency reference for the photon-pair source [36] and the second for the memory preparation [23]. Their frequency and amplitude are varied by double-pass acousto-optic modulators (AOMs) driven by an arbitrary waveform generator (Signadyne). After the AOMs, the beams are coupled into polarization maintaining single-mode fibers and out-coupled in two separated optical benches hosting the source and the cryostat (closed cycle cryogenic cooler, Oxford V14), which is exploited to cool the $Pr^{3+}:Y_2SiO_5$ crystal down to 2.8 K.

The heralded single photons are obtained from the photon-pair source, whose detailed description is given in Ref. [36]. A cw pump beam at 426.2 nm, modulated by an AOM, produces photons at 606 nm (signal) and 1436 nm (idler) by SPDC in a temperature-stabilized periodically poled lithium niobate (PPLN) crystal. A bow-tie cavity surrounding the crystal enhances the SPDC process for the resonant frequencies. The cavity is stabilized with the reference beam at 606 nm, to ensure the signal resonance with the $Pr^{3+}:Y_2SiO_5$ crystal. To maintain the cavity resonant with the idler, the pump frequency is locked using light at the idler frequency created by difference frequency generation of the pump and the 606 nm reference beam passing through the same PPLN crystal. The double resonance allows a very efficient suppression of the redundant spectral modes due to the so-called clustering effect [36]. The photon-pairs' spectrum is thus composed of a main cluster and two secondary clusters separated by 44.5 GHz, each containing four longitudinal modes [36]. In order to operate in the single-mode regime, the heralding telecom photons are filtered by a home-made filter cavity (linewidth ≈80 MHz and free spectral range (FSR) ≈16.8 GHz). They are then coupled into a single mode fiber and detected by an InGaAs single photon detector (SPD, IdQuantique id220, detection efficiency $\eta_{d,i} = 10$ % and 400 Hz dark count rate). The heralded 606 nm photons are filtered with an etalon (linewidth ≈ 10 GHz and FSR ≈60 GHz), resulting in the mere suppression of the secondary clusters. They are then sent to the crystal via a single mode fiber. The optical transmission of the signal (idler) photon from the output of the bow-tie cavity to the cryostat (SPD) is $\eta_s = 0.18$ ($\eta_i = 0.22$). To optimize the detection of the stored and retrieved photons, we switch off the pump beam using the AOM after the detection of an idler photon, thus interrupting the creation of new photon pairs. The correlation time of the photon pair is measured from the idler-signal cross-correlation function $G^{(2)}_{s,i}(t)$ to be $\tau_c = 108$ ns, corresponding to a photon bandwidth of $\delta\nu = 2.3$ MHz (1.84 MHz) for the signal (idler) photons [36].

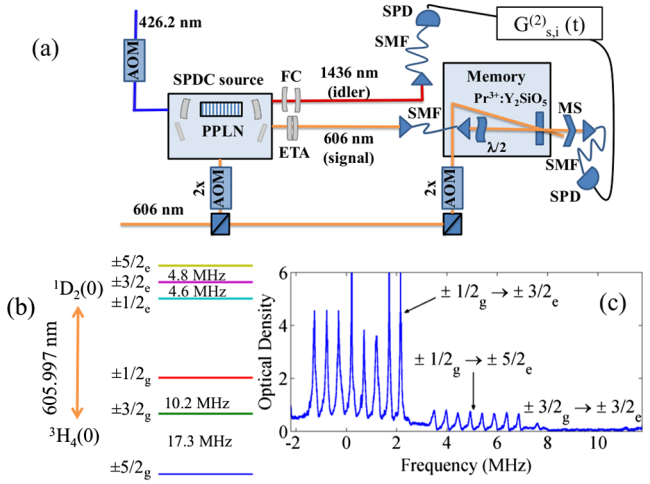

FIG. 1 (color online). (a) Experimental setup. AOM, acousto-optic modulator (2x when double pass); FC, filter cavity; ETA, etalon; SMF, single-mode fiber; MS, mechanical shutter; SPD, single photon detector; $\lambda/2$, half-wave plate. (b) Energy level scheme of Pr^{3+} in Y_2SiO_5 restricted to the fundamental levels of the ground $^3H_4$ and the excited $^1D_2$ manifolds. (c) Example of AFC with $\Delta = 500$ kHz.

Our storage device is a 3 mm thick Y_2SiO_5 sample doped with a Pr^{3+} concentration of 0.05%. The relevant optical transition is at 605.977 nm with a measured absorption coefficient of $\alpha = 23$ cm^{-1} and an inhomogeneous linewidth of 5 GHz [23]. A half-wave plate ($\lambda/2$) ensures the polarization of the photons is aligned close to the optical D_2 axis of the crystal, in order to maximize the absorption. To prevent noise from the strong preparation beam polluting the single photon mode, we use two different optical paths with an angle of 2.5 degrees. The maximum power in the preparation mode before the cryostat window is 6 mW and the beam diameter at the crystal is 150 μm. The beam diameter for the input mode is 50 μm. The single photon mode is directed to a Si-SPD (Excelitas Technologies, efficiency $\eta_{d,s} = 32\%$ and 10 Hz dark counts) via a single mode fiber.

To prepare the memory we follow the procedure thoroughly described in Refs. [23,38]. We prepare a transparency window within the inhomogeneously broadened Pr^{3+} absorption at 606 nm by sweeping the laser frequency by 12 MHz. The narrow transparency window contributes to select only one mode among the four

remaining in the main-cluster of the source spectrum which are separated by 412 MHz [36]. Afterwards we tailor a single class AFC on the $\pm 1/2_g - \pm 3/2_e$ transition by first burning back atoms with pulses at frequencies differing by Δ and then performing a cleaning sweep in the region of the $\pm 3/2_g - \pm 3/2_e$ transition [see Fig. 1(b)]. To ensure the efficient absorption of the photons by the periodic structure, the total comb width is set to 3.5 MHz [see Fig. 1(c) for an example with $\Delta = 500$ kHz]. With the present preparation procedure (which lasts for 300 ms) we are able to tailor spectral features as narrow as 60 kHz. The input photon frequency is selected to be resonant with the $\pm 1/2_g - \pm 3/2_e$ transition. Note that the procedure used for the comb preparation empties the $\pm 3/2_g$ ground state. The $\pm 3/2_g - \pm 3/2_e$ transition could then be directly used to transfer optical excitations to spin excitations, as demonstrated in Refs. [22,23] for bright pulses.

The arrival times of the photons to the detectors are recorded with a time-stamping card (Signadyne) and used to reconstruct the second-order cross-correlation function between the signal and idler $G^{(2)}_{s,i}(t)$. A figure of merit for the nonclassical nature of the photon correlations is the normalized cross-correlation function [3,30]

$$g^{(2)}_{s,i} = \frac{p_{s,i}}{p_s p_i}, \tag{1}$$

where p_s (p_i) is the probability to detect a signal (idler) photon and $p_{s,i}$ the probability to detect a coincidence in a time window $\Delta t_d = 400$ ns centered at zero time delay. All the results presented in this Letter are from raw data, without any background or dark count subtraction, unless otherwise stated.

We first characterize the input heralded single photon by sending it through the memory crystal when only a transparency window is created [see blue histogram centered at zero time delay in Fig. 2(a)]. The values of $g^{(2)}_{s,i}$ as a function of the pump power are plotted in Fig. 2(b). Despite the expected decrease for increased pump power due to the production of multiple pairs [39], the values remain well above the classical limit of 2 (dotted line) for two-mode squeezed states.

In order to unambiguously confirm the nonclassical nature of the correlation, we also measure the marginal auto-correlation function for the signal and idler mode, $g^{(2)}_{s,s}$ and $g^{(2)}_{i,i}$. We find, at the pump power of 5 mW, $g^{(2)}_{s,s} = 1.14 \pm 0.03$ and $g^{(2)}_{i,i} = 1.07 \pm 0.02$, leading to strong violation of the Cauchy-Schwarz inequality in the form $R = (g^{(2)}_{s,i})^2/(g^{(2)}_{i,i} \times g^{(2)}_{s,s}) = 61 \pm 2 \not\leq 1$ which proves nonclassical correlations without any assumption on the created state (see Supplemental Material [40]).

The detected coincidence rate (within Δt_d) is $C_d = (0.83 \pm 0.14)$ Hz/mW. From this value, we infer the generated coincidence rate C_g at the output of the source

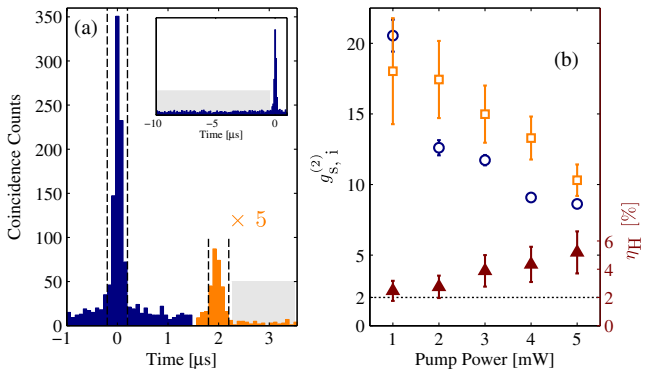

FIG. 2 (color online). (a) $G^{(2)}_{s,i}(t)$ histogram without (blue) and with (orange) AFC. The preprogrammed storage time is 2 μs and the power of the 426.2 nm pump is 2 mW. The time-bin size is 5 ns. The dashed lines and shaded area define the detection windows for the coincidences ($\Delta t_d = 400$ ns) and noise, respectively, used to compute $g^{(2)}_{s,i}$. (b) The $g^{(2)}_{s,i}$ values as a function of the pump power for the AFC echo (empty squares) are compared to those for the input photons (empty circles). The heralding efficiencies η_H are also reported (filled triangles).The integration times range between 30 and 60 minutes. The error bars are evaluated from the raw number of counts assuming Poissonian statistics. The dotted line corresponds to the classical limit $g^{(2)}_{s,i} = 2$ for two-mode squeezed states.

cavity $C_g = C_d/(\eta_i \eta_{d,i} \eta_s \eta_{\text{loss}} \eta_{d,s}) = 2.8$ kHz/mW, where $\eta_{\text{loss}} = 0.225$ is the transmission from the input of the cryostat to the signal SPD, including the duty cycle of the memory (50%, see Supplemental Material [40]). We can also evaluate the heralding efficiency in front of the cryostat, $\eta_H = p_{s,i}/(p_i \times \eta_{d,s} \times \eta_{\text{loss}})$, whose values as a function of pump power are plotted in Fig. 2(b) (full triangles). Note that η_H is mainly limited by η_s and dark counts in the heralding SPD. Subtracting the contribution of the 1436 nm detector dark counts we find corrected heralding efficiencies almost constant, $\eta_H{}^{DC} \approx 6.3\%$ (35% at the output of the source cavity), over the whole range of pump powers investigated. Finally, we estimate that more than 95% of the heralded signal photons detected after the crystal are resonant with the atoms (see Supplemental Material [40]) [41].

Once the nonclassical nature of the input photons propagating through the transparency window is demonstrated, we prepare the AFC and reconstruct the $G^{(2)}_{s,i}(t)$ function for the stored and retrieved photons. Figure 2(a) includes the coincidence histogram when an AFC is producing a collective re-emission at a delay of $\tau = 2$ μs (orange trace). The values of $g^{(2)}_{s,i}$ for the AFC echo as a function of the pump power are reported in Fig. 2(b) (empty squares). The count rate in the region of the AFC echo is $C = (0.043 \pm 0.03)$ Hz/mW. We observe that the echoes exhibit $g^{(2)}_{s,i}$ values higher than the input photons. We attribute this unexpected effect to the fact that the AFC acts as a temporal filter [42] for nonresonant noise arising from the SPDC source. Since the SPDC pump laser is

turned off after the detection of an idler photon, the AFC delays the signal to a region free of broadband noise, thus increasing the $g^{(2)}_{s,i}$. A more quantitative analysis of this effect is presented in the Supplemental Material [40]. When the pump power decreases, the detection of the echo is limited by the detector dark counts. This gives rise to a saturation of the echo $g^{(2)}_{s,i}$ values which hides the filtering effect of the storage.

In view of applications in temporally multimode quantum memories with on-demand readout, the preprogrammed delay τ must be tunable to allow the application of control pulses transferring the excitation to the spin states [23]. Thus, we changed the spectral periodicity Δ of the AFC to obtain increased delays. Figure 3(a) shows the coincidence histograms in the region of the AFC echo occurring at different predetermined storage times. The AFC storage efficiency, η_{AFC}, is estimated by comparing the number of counts of the input propagating through the transparency window and the echo; it decreases for longer delays, as shown in Fig. 3(b), denoting a reduction of the comb finesse [18]. We note that the AFC efficiency with single photons does not decrease with respect to the storage of bright or weak coherent pulses of similar durations (the different cases together with a theoretical evaluation are compared in the Supplemental Material [40]). This confirms that there is no significant frequency jitter for the single photons. We could reach AFC storage times of 4.5 μs, while preserving nonclassical correlations [see Fig. 3(c)]. As we stop the production of pairs after the detection of a telecom photon, the region where the echo lies should not be affected by unconditional noise coming from the source (see Supplemental Material [40]). Thus, despite the reduction in the AFC efficiency, the echo should exhibit constant values of $g^{(2)}_{s,i}$ for increasing storage times. As a matter of fact, the decrease in the $g^{(2)}_{s,i}$ values while increasing the storage time is less pronounced than the drop of the AFC efficiency [compare the diamonds in panels (b) and (c) of Fig. 3] and we attribute the reduction to the limitation given by the detector dark counts.

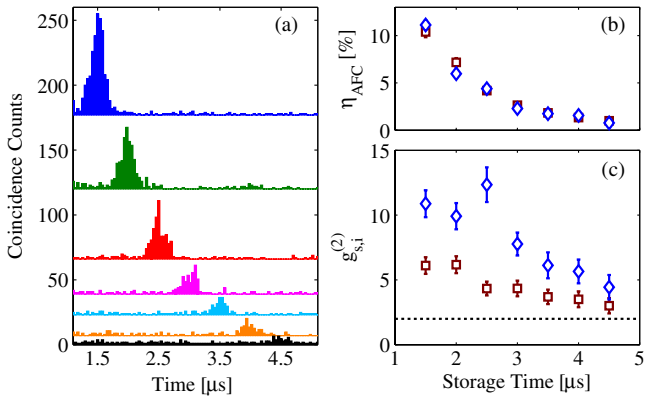

FIG. 3 (color online). (a) AFC echoes at different predetermined storage times observed in coincidence histograms measured at 2 mW pump power (integration time is 40 minutes and the time-bin size is 5 ns). The curves are vertically shifted for clarity. (b) and (c), AFC efficiency and $g^{(2)}_{s,i}$ (calculated in a 400 ns window) of the AFC echo as a function of the storage time. Diamonds: filter cavity in the heralding photon path; squares: filter cavity removed from the heralding photon path. The error bars are evaluated from the raw counts assuming Poissonian statistics. The dotted line corresponds to the classical limit $g^{(2)}_{s,i} = 2$ for two-mode squeezed states.

We also report the values of η_{AFC} and $g^{(2)}_{s,i}$ measured without the filter cavity in the idler arm. The efficiencies in the two cases agree within the experimental error. On the contrary, despite the factor 2 gain in the raw number of counts thanks to the reduced passive losses, the $g^{(2)}_{s,i}$ without filter cavity decreases due to the frequency multimodality of the source [36]. In fact, among the four modes coexisting in the main cluster, only one is resonant with the AFC. The nonresonant modes in the idler arm join the start signals for the coincidence histogram without corresponding stops (the Pr^{3+} absorption acts as a filter for the nonresonant mode in the 606 nm arm), thus decreasing the heralding efficiency and contributing to the noise increase. Note that frequency multiplexed quantum light storage could be obtained by creating several AFCs at different frequencies separated by the SPDC cavity FSR [24].

Our experiment could be extended to the storage of entangled qubits (e.g., entangled in energy time [30] or in polarization with a suitable modification of the pair source). Alternatively, by doubling the setup, the demonstrated light matter quantum correlations would enable heralded entanglement between remote crystals [37]. For the two cases, the visibility V of the two-photon interference would be given by the measured $g^{(2)}_{s,i}$ of the stored and retrieved photons as (assuming uncorrelated background) $V = (g^{(2)}_{s,i} - 1)/(g^{(2)}_{s,i} + 1)$ [43,44]. For the values of $g^{(2)}_{s,i}$ measured in this work, this would lead to visibilities between 0.67 and 0.9. In addition, for the latter experiment, the demonstrated storage time would allow entanglement between crystals separated by km range distances.

In conclusion, we have demonstrated the reversible mapping of heralded single photons to collective optical atomic excitations in a praseodymium doped crystal. We observed an increase of nonclassical correlations between signal and idler photons during the storage, thanks to a temporal filtering effect due to the AFC. Storage times up to 4.5 μs while preserving quantum correlations were observed, more than 20 times longer than previous solid state experimental realizations. Furthermore, the transition used would readily allow the transfer of the excitation to the ground state to obtain long-lived spin-wave storage of the quantum state of light, provided that the noise induced by the control beams can be sufficiently reduced.

We thank M. Afzelius and F. Bussières for interesting discussions. We acknowledge financial support by the

European projects CHIST-ERA QScale and FP7-CIPRIS (MC ITN-287252), by the ERC Starting grant QuLIMA and by the Spanish MINECO OQISAM project (FIS2012-37569). M. M. acknowledges the Beatriu de Pinós program (2010BP B0014) for financial support.

*Present address: Physics Department, University of Otago, New Zealand
†margherita.mazzera@icfo.es

[1] K. Hammerer, A. S. Sørensen, and E. S. Polzik, Rev. Mod. Phys. **82**, 1041 (2010).
[2] H.-J. Briegel, W. Dür, J. I. Cirac, and P. Zoller, Phys. Rev. Lett. **81**, 5932 (1998).
[3] N. Sangouard, C. Simon, H. de Riedmatten, and N. Gisin, Rev. Mod. Phys. **83**, 33 (2011).
[4] H. P. Specht, C. Nölleke, A. Reiserer, M. Uphoff, E. Figueroa, S. Ritter, and G. Rempe, Nature (London) **473**, 190 (2011).
[5] T. Chanelière, D. N. Matsukevich, S. D. Jenkins, S.-Y. Lan, T. A. B. Kennedy, and A. Kuzmich, Nature (London) **438**, 833 (2005).
[6] C. W. Chou, H. de Riedmatten, D. Felinto, S. V. Polyakov, S. J. van Enk, and H. J. Kimble, Nature (London) **438**, 828 (2005).
[7] J. Simon, H. Tanji, J. K. Thompson, and V. Vuletic, Phys. Rev. Lett. **98**, 183601 (2007).
[8] A. G. Radnaev, Y. O. Dudin, R. Zhao, H. H. Jen, S. D. Jenkins, A. Kuzmich, and T. A. B. Kennedy, Nat. Phys. **6**, 894 (2010).
[9] H. Zhang, X.-M. Jin, J. Yang, H.-N. Dai, S.-J. Yang, T.-M. Zhao, J. Rui, Y. He, X. Jiang, F. Yang, G.-S. Pan, Z.-S. Yuan, Y. Deng, Z.-B. Chen, X.-H. Bao, S. Chen, B. Zhao, and J.-W. Pan, Nat. Photonics **5**, 628 (2011).
[10] B. Julsgaard, J. Sherson, J. I. Cirac, J. Fiurášek, and E. S. Polzik, Nature (London) **432**, 482 (2004).
[11] M. D. Eisaman, A. André, F. Massou, M. Fleischhauer, A. S. Zibrov, and M. D. Lukin, Nature (London) **438**, 837 (2005).
[12] K. F. Reim, P. Michelberger, K. C. Lee, J. Nunn, N. K. Langford, and I. A. Walmsley, Phys. Rev. Lett. **107**, 053603 (2011).
[13] M. Hosseini, G. Campbell, B. M. Sparkes, P. K. Lam, and B. C. Buchler, Nat. Phys. **7**, 794 (2011).
[14] W. Tittel, M. Afzelius, T. Chanelière, R. L. Cone, R. L. S. Kröll, S. A. Moiseev, and M. Sellars, Laser Photonics Rev. **4**, 244 (2010).
[15] R. M. Macfarlane, J. Lumin. **100**, 1 (2002).
[16] M. P. Hedges, J. J. Longdell, Y. Li, and M. J. Sellars, Nature (London) **465**, 1052 (2010).
[17] M. Sabooni, Q. Li, S. Kröll, and L. Rippe, Phys. Rev. Lett. **110**, 133604 (2013).
[18] H. de Riedmatten, M. Afzelius, M. U. Staudt, C. Simon, and N. Gisin, Nature (London) **456**, 773 (2008).
[19] M. Afzelius, C. Simon, H. de Riedmatten, and N. Gisin, Phys. Rev. A **79**, 052329 (2009).
[20] I. Usmani, M. Afzelius, H. de Riedmatten, and N. Gisin, Nat. Commun. **1**, 12 (2010).
[21] M. Bonarota, J.-L. Le Gouët, and T. Chanelière, New J. Phys. **13**, 013013 (2011).
[22] M. Afzelius, I. Usmani, A. Amari, B. Lauritzen, A. Walther, C. Simon, N. Sangouard, J. Minář, H. de Riedmatten, N. Gisin, and S. Kröll, Phys. Rev. Lett. **104**, 040503 (2010).
[23] M. Gündoğan, M. Mazzera, P. M. Ledingham, M. Cristiani, and H. de Riedmatten, New J. Phys. **15**, 045012 (2013).
[24] N. Sinclair, E. Saglamyurek, H. Mallahzadeh, J. A. Slater, M. George, R. Ricken, M. P. Hedges, D. Oblak, C. Simon, W. Sohler, and W. Tittel, arXiv:1309.3202.
[25] M. Sabooni, F. Beaudoin, A. Walther, N. Lin, A. Amari, M. Huang, and S. Kröll, Phys. Rev. Lett. **105**, 060501 (2010).
[26] T. Chanelière, J. Ruggiero, M. Bonarota, M. Afzelius, and J.-L. Le Gouët, New J. Phys. **12**, 023025 (2010).
[27] M. Gündoğan, P. M. Ledingham, A. Almasi, M. Cristiani, and H. de Riedmatten, Phys. Rev. Lett. **108**, 190504 (2012).
[28] Z.-Q. Zhou, W.-B. Lin, M. Yang, C.-F. Li, and G.-C. Guo, Phys. Rev. Lett. **108**, 190505 (2012).
[29] N. Timoney, I. Usmani, P. Jobez, M. Afzelius, and N. Gisin, Phys. Rev. A **88**, 022324 (2013).
[30] C. Clausen, I. Usmani, F. Bussières, N. Sangouard, M. Afzelius, H. de Riedmatten, and N. Gisin, Nature (London) **469**, 508 (2011).
[31] E. Saglamyurek, N. Sinclair, J. Jin, J. A. Slater, D. Oblak, F. Bussières, M. George, R. Ricken, W. Sohler, and W. Tittel, Nature (London) **469**, 512 (2011).
[32] I. Usmani, C. Clausen, F. Bussières, N. Sangouard, M. Afzelius, and N. Gisin, Nat. Photonics **6**, 234 (2012).
[33] C. Clausen, F. Bussières, M. Afzelius, and N. Gisin, Phys. Rev. Lett. **108**, 190503 (2012).
[34] E. Saglamyurek, N. Sinclair, J. Jin, J. A. Slater, D. Oblak, F. Bussières, M. George, R. Ricken, W. Sohler, and W. Tittel, Phys. Rev. Lett. **108**, 083602 (2012).
[35] G. Heinze, C. Hubrich, and T. Halfmann, Phys. Rev. Lett. **111**, 033601 (2013).
[36] J. Fekete, D. Rieländer, M. Cristiani, and H. de Riedmatten, Phys. Rev. Lett. **110**, 220502 (2013).
[37] C. Simon, H. de Riedmatten, M. Afzelius, N. Sangouard, H. Zbinden, and N. Gisin, Phys. Rev. Lett. **98**, 190503 (2007).
[38] M. Nilsson, L. Rippe, S. Kröll, R. Klieber, and D. Suter, Phys. Rev. B **70**, 214116 (2004).
[39] M. Förtsch, J. Fürst, C. Wittmann, D. Strekalov, A. Aiello, M. V. Chekhova, C. Silberhorn, G. Leuchs, and C. Marquardt, Nat. Commun. **4**, 1818 (2013).
[40] See Supplemental Material at http://link.aps.org/supplemental/10.1103/PhysRevLett.112.040504 for document providing details about the experimental setup, the characterization of the AFC storage efficiency, the second-order auto-correlation of signal and idler photons, and the second-order cross-correlation measurements between signal and idler photons as a function of polarization.
[41] F. Wolfgramm, Y. A. de Icaza Astiz, F. A. Beduini, A. Cerè, and M. W. Mitchell, Phys. Rev. Lett. **106**, 053602 (2011).
[42] D. L. McAuslan, L. R. Taylor, and J. J. Longdell, Appl. Phys. Lett. **101**, 191112 (2012).
[43] H. de Riedmatten, J. Laurat, C. W. Chou, E. W. Schomburg, D. Felinto, and H. J. Kimble, Phys. Rev. Lett. **97**, 113603 (2006)
[44] J. Laurat, K. S. Choi, H. Deng, C. W. Chou, and H. J. Kimble, Phys. Rev. Lett. **99**, 180504 (2007).